THE JOURNAL OF BIOLOGICAL CHEMISTRY VOL. 286, NO. 6, pp. 4511–4516, February 11, 2011
© 2011 by The American Society for Biochemistry and Molecular Biology, Inc. Printed in the U.S.A.

Structural Basis of Tumor Suppressor in Lung Cancer 1 (TSLC1) Binding to Differentially Expressed in Adenocarcinoma of the Lung (DAL-1/4.1B)*

Received for publication, August 10, 2010, and in revised form, November 27, 2010 Published, JBC Papers in Press, December 3, 2010, DOI 10.1074/jbc.M110.174011

Robert D. Busam[‡1], Ann-Gerd Thorsell[‡], Alex Flores[‡], Martin Hammarström[‡], Camilla Persson[‡], Björn Öbrink[§2], and B. Martin Hallberg[§3]

From the [‡]Structural Genomics Consortium, Department of Medical Biochemistry and Biophysics and the [§]Department of Cell and Molecular Biology, Karolinska Institutet, SE-17177 Stockholm, Sweden

Perturbed cell adhesion mechanisms are crucial for tumor invasion and metastasis. A cell adhesion protein, TSLC1 (tumor suppressor in lung cancer 1), is inactivated in a majority of metastatic cancers. DAL-1 (differentially expressed in adenocarcinoma of the lung protein), another tumor suppressor, binds through its FERM domain to the TSLC1 C-terminal, 4.1 glycophorin C-like, cytoplasmic domain. However, the molecular basis for this interaction is unknown. Here, we describe the crystal structure of a complex between the DAL-1 FERM domain and a portion of the TSLC1 cytoplasmic domain. DAL-1 binds to TSLC1 through conserved residues in a well defined hydrophobic pocket in the structural C-lobe of the DAL-1 FERM domain. From the crystal structure, it is apparent that Tyr[406] and Thr[408] in the TSLC1 cytoplasmic domain form the most important interactions with DAL-1, and this was also confirmed by surface plasmon resonance studies. Our results refute earlier exon deletion experiments that indicated that glycophorin C interacts with the α-lobe of 4.1 FERM domains.

Immunoglobulin superfamily cell adhesion molecules are a diverse group of proteins that consist of >100 members in vertebrates (1). These adhesion receptors are involved in cell-cell and cell-matrix interactions. Additionally, they are important in differentiation, proliferation, and cell motility (2–4). Decreased or loss of function of these molecules can result in disruption to cell adhesion, sometimes resulting in metastasis. TSLC1 (tumor suppressor in lung cancer 1) is an immunoglobulin superfamily cell adhesion molecule that was originally identified as a lung tumor suppressor (5). Further studies have established its role in metastasis, tumor suppression, and spermatogenesis (6, 7). TSLC1 is involved in cell-cell adhesion and consists of three extracellular Ig-like C2-type domains, a transmembrane region, and a cytoplasmic domain (8). The cytoplasmic domain, which is critical in tumor suppressor activity (9), contains a conserved protein 4.1 binding motif and binds differentially expressed in adenocarcinoma of the lung protein (DAL-1/4.1B) (10).

DAL-1 is a tumor suppressor in lung cancer and homologous to proteins in the protein 4.1 superfamily (11). It has been implicated in a variety of meningiomas and carcinomas and is a proposed target for prostate cancer therapy (12). Members of this large family play a role in cell adhesion and the structure and regulation of the membrane skeleton (13). These proteins are involved in linking cytoskeletal proteins to the membrane via a 4.1 protein/ezrin/radixin/moesin (FERM) domain (14). This domain structure has a cloverleaf architecture with three distinct lobes, as first seen from the crystal structure of protein 4.1R (15). Additional FERM domain structures of radixin, moesin, merlin, talin, ezrin, and focal adhesion kinase maintain a similar topology (16–21). DAL-1 is an 1087-amino acid protein consisting of an N-terminal FERM domain (residues 110–391), a hydrophilic FERM adjacent domain (residues 394–513), spectrin and actin binding domain (residues 514–860), and a C-terminal domain (residues 861–1083) according to Uniprot entry Q9Y2J2 (22). The DAL-1 FERM domain binds TSLC1, 14-3-3 proteins, and protein arginine *N*-methyltransferases (10, 23, 24). Exon deletion studies indicated that the α-lobe of 4.1 FERM domains interacts with the cytoplasmic domain of glycophorin C (25). This is in contrast to other FERM domains that predominantly form analogous interactions through their C-lobe.[4]

The cytoplasmic domain of TSLC1 contains a conserved sequence of 10 amino acids that matches a proposed consensus protein 4.1 binding motif, $RXK(X)_{0-4}GXY(X)_3E$ (10). Here, we describe the structure of the FERM domain of human DAL-1 in complex with a peptide corresponding to the consensus protein 4.1 binding motif of the cytoplasmic C-

* The Structural Genomics Consortium is a registered charity (no. 1097737) that receives funds from the Canadian Institutes for Health Research, the Canada Foundation for Innovation, Genome Canada through the Ontario Genomics Institute, GlaxoSmithKline, Karolinska Institutet, the Knut and Alice Wallenberg Foundation, the Ontario Innovation Trust, the Ontario Ministry for Research and Innovation, Merck and Co., Inc., the Novartis Research Foundation, the Swedish Agency for Innovation Systems, the Swedish Foundation for Strategic Research, and the Wellcome Trust.

The atomic coordinates and structure factors (codes 2HE7 and 3BIN) have been deposited in the Protein Data Bank, Research Collaboratory for Structural Bioinformatics, Rutgers University, New Brunswick, NJ (http://www.rcsb.org/).

[1] Supported by the Wenner-Gren Foundations.

[2] Supported by grants from the Swedish Research Council (Grant 2007-3772) and the Swedish Cancer Foundation (Grant 07 0629).

[3] Junior Research Fellow of The Swedish Research Council (Grant 2006-4211). To whom correspondence should be addressed. E-mail: Martin.Hallberg@ki.se.

[4] The abbreviations used are: C-lobe, C-terminal lobe; N-lobe, N-terminal lobe; GPC, glycophorin C; FERM, 4.1 protein/ezrin/radixin/moesin; ICAM, inter-cellular adhesion molecule.

terminal domain of TSLC1. This is the first peptide co-crystal structure of a 4.1 superfamily member. The crystal structure reveals that DAL-1 FERM domain binds TSLC1 in the C-lobe and not in the α-lobe, thereby refuting earlier claims of an idiosyncratic glycophorin C binding mode for the 4.1 superfamily FERM domains.

EXPERIMENTAL PROCEDURES

Cloning, Expression, and Purification of DAL-1—The sequence of the FERM domain of DAL-1 (residues 106–397) (gi: 13544009) were cloned by ligation-independent cloning into a pET-28 based expression vector incorporating a tobacco etch virus-cleavable N-terminal His tag fusion (pNIC-Bsa4; gi: EF198016). After transformation and liquid culture growth using standard methods, recombinant expression of DAL-1 was induced at 291 K by addition of 0.5 mM isopropyl-β-D-thiogalactopyranoside to Terrific broth supplemented with 8g/liter 87% glycerol. After harvesting, DAL-1 was purified using immobilized metal affinity chromatography with a 1 ml HiTrap chelating HP column followed by gel filtration on a Superdex 200 column (GE Healthcare). Isolated protein was unstable without 500 mM betaine present in buffers (discovered through Thermofluor buffer-screening assays (26)). Pooled fractions were collected and concentrated to a concentration of 44.7 mg/ml in buffer A (20 mM HEPES pH 7.5, 300 mM NaCl, 10% glycerol, 0.5 mM tris(2-carboxyethyl)-phosphine, 500 mM betaine).

Crystallization and X-ray Data Collection—Prior to crystallization, DAL-1 was diluted to a final concentration of 12 mg/ml in buffer A. DAL-1 crystallized at room temperature in 20% ethanol and 10 mM Tris (pH 8.2) utilizing the hanging drop vapor diffusion method. 1.0 μl of protein solution was added to 1.0 μl of well solution, centered on the coverslip. Needles (30 × 50 × 500 micron) grew within 1 day, and diffraction data were collected at the European Synchrotron Radiation Facility beam line ID-23.1. A peptide corresponding to the part of the TSLC1 cytoplasmic domain involved in binding DAL-1 (10), ^{400}ARHKGTYFTHEA (Genscript), was dissolved to 50 mg/ml in buffer (0.1 M Tris pH 8.5, 15% ethanol). An aliquot of this solution was tested with pH paper and found to be acidic (pH < 4.0). pH was adjusted to 7.5 with 1 M Tris (pH 8.5) buffer. 0.4 μl of peptide solution was added to room temperature drops containing DAL-1 crystals grown in 15% ethanol and 10 mM Tris (pH 8.2). After 1 h, the soaked crystals were flash frozen in liquid nitrogen after being swept through precipitant solution with 15% 2,3-butanediol added. The DAL-1/TSLC1 data were collected at ESRF beam line ID14.4 (Table 1).

Structure Determination—The crystal structure of the DAL-1 protein was determined by molecular replacement using Protein Data Bank code 1GG3 (15) and the program PHASER in the CCP4 program suite (27, 28). The DAL-1/TSLC1 model was solved by molecular replacement using the DAL-1 structure as a starting model. In both cases, the data were scaled and integrated with XDS/XSCALE (29). The models were built into the electron density maps using COOT (30) and refined using REFMAC5 (31). See Table 1 for final statistics.

Surface Plasmon Resonance—Binding experiments were performed with a BIAcore 2000 instrument (GE Healthcare). N-terminally biotinylated peptides were immobilized by binding to streptavidin on streptavidin sensor chips (GE Healthcare). The N-terminally biotinylated peptides had the following sequences: WT, GSGSGSARHKGTYFTHEA; Y406A, GSGSGSARHKGTAFTHEA; T408A, GSGSGSARHKGTYFAHEA; Y406A,T408A, GSGSGSARHKGTAFAHEA; and scrambled, GSGSGSAGHATFAHREAK (all from GL Biochem, Shanghai, China). The peptides, at a concentration of 50 μg/ml in HBS (10 mM Hepes, pH 7.4; 0.15 M NaCl), were immobilized on streptavidin chips by injection in separate lanes at a flow rate of 5 μl/min for 2 × 7 min. After immobilization, the lanes were washed by two injections of 4 M guanidine-HCl/HBS (pH 7.4) for 2 min and one injection of 0.25% P20/HBS for 2 min, at a flow rate of 20 μl/min. The levels of stably immobilized peptides were 470–530 response units per lane. All interaction analyses were performed at 298 K at a flow rate of 20 μl/min, in HBS/0.005% P20/0.5 mM tris(2-carboxyethyl)phosphine/0.5 M betaine. DAL-1 at concentrations 0.1–1.0 mg/ml were injected for 3 min, followed by buffer injection for 5 min. After each binding cycle, the chip surface was regenerated with two cycles of 4 M guanidine-HCl/HBS and one cycle of 0.25% P20/HBS. Corrected binding profiles (sensorgrams) for DAL-1 were obtained by subtracting the response in the reference lane (scrambled peptide) from the response in the binding lanes (WT and mutant peptides). Data modification including scale transformation and background subtraction was performed with the program BIAevaluation 4.1 (GE Healthcare).

Figure Preparation—The figures were created with PyMOL (32). The conserved surface residues were determined by ConSurf (33) using default parameters (multiple sequence alignment using MUSCLE; maximum of 50 homologues from SWISS-PROT; 1 PSI-BLAST, 0.001 PSI-BLAST value cut-off; JTT model of substitution). The electrostatic surface potential was calculated using ABPS (34) and contoured at ±10 kT/e (where k is Boltzmann's constant, T is the absolute temperature, and e is the unit electron charge). The alignment of peptides bound to the FERM domain were done using the Secondary Structure Matching server (35) by aligning main chain atoms of the β-strand 5βC (residues 334–344) and α-helix α1C (residues 368–390) of DAL-1 with those of the corresponding FERM domain.

Data Deposition—Atomic coordinates and structure factors for DAL-1 and DAL-1·TSLC1 have been deposited in the RCSB Protein Data Bank (accession codes 2HE7 and 3BIN).

RESULTS AND DISCUSSION

Overall Structure of DAL-1 and DAL-1·TSLC1 Complex—The DAL-1 and DAL-1·TSLC1 structures were solved at 2.0 and 2.3 Å resolution, respectively (Table 1). These structures adopt the three-lobed, clover leaf architecture as typically seen in FERM domain structures such as radixin, moesin, merlin, talin, ezrin, and focal adhesion kinase (16–21). The protein consists of three structural lobes: N-lobe, α-lobe, and

TABLE 1
Data measurement and refinement statistics

	DAL-1	DAL-1·TSLC1
Resolution (Å)	30.0-2.0 (2.1-2.0)	30.0-2.3 (2.36-2.3)
Space group	$P6_5$	$P6_5$
Unit cell (Å; $a = b, c$)	135.5, 49.8	135.0, 52.5
No. of observed reflections	390,998 (52,927)	85,735 (6184)
No. of unique reflections	35,521 (4784)	23,489 (1649)
Completeness (%)	99.4 (100.0)	99.3 (100.0)
Redundancy	11.0 (11.1)	3.65 (3.75)
$\langle I/\sigma(I)\rangle$	21.1 (4.8)	18.9 (3.0)
R_{merge} [a]	0.08 (0.561)	0.05 (0.42)
No. of atoms		
Protein	2449	2411
Water	247	144
Average thermal factor (Å^2)		
Protein	34.7	46.4
Peptide		71.0
Water	43.6	50.4
r.m.s.d. from ideality [b]		
Bond lengths (Å)	0.021	0.022
Bond angles	1.74°	1.81°
R_{work} [c]	0.19 (0.26)	0.18 (0.26)
R_{free} [c]	0.22 (0.28)	0.23 (0.31)

[a] $R_{merge} = \Sigma_{hkl}\Sigma_i|I_{i(hkl)} - \langle I_{(hkl)}\rangle|/\Sigma_{hkl}\Sigma_i I_{i(hkl)}$ where $I_{i(hkl)}$ is the observed intensity and $\langle I_{(hkl)}\rangle$ is the average intensity.
[b] r.m.s.d., root mean square deviation.
[c] $R_{factor} = \Sigma||F_o| - |F_c||/\Sigma|F_o|$ where F_o and F_c are the observed and calculated structure factors, respectively. R_{free} is the cross-validation R_{factor} calculated for 5% of the reflections omitted during the refinement process.

C-lobe (Fig. 1*A*). The N-lobe is formed by a five-strand anti-parallel β-sheet that partially wraps around a central helix. The α-lobe is entirely α-helical, containing four loosely packed helices, one of which interacts with the N-lobe. The C-lobe consists of an anti-parallel seven-stranded β-sandwich, terminating in a C-terminal α-helix, which packs between β5C and β1C. The TSLC1 peptide binds to the α1C helix and the β5C strand (Fig. 1, *A* and *B*). Secondary structure matching (35) of the apo form to the TSLC1 peptide bound structure (DAL-1·TSLC1) results in a core root mean square deviation of only 0.47 Å, but there are significant structural shifts close to the bound peptide.

TSLC1 Peptide Binding and Recognition—TSLC1 contains a C-terminal cytoplasmic domain that consists of 47 amino acids shown to be important in tumor suppression (9). Secondary structure prediction suggests this domain is highly flexible with little to no structure (data not shown). The peptide bound to DAL-1 consists of 12 residues (ARHKGTYFTHEA) corresponding to the consensus 4.1 binding motif region of the TSLC1 C-terminal domain (residues 400–411). This peptide binds DAL-1 at the interface between helix α1C and β-strand β5C, forming a short antiparallel β-sheet with β5C (Fig. 1, *A* and *B*). Upon TSLC1 binding, the neighboring C-terminal residues of DAL-1 undergo a significant shift; the Arg^{388} guanidinium group moves ~5.8 Å from the apo position to form a salt bridge with Glu^{410}. Leu^{389} and Leu^{390} are translated ~35° away from the binding site (Fig. 2*C*). In the binding site, there is clear electron density in our crystal structure for seven residues (GTYFTHE). These seven residues make up the part of the peptide that is close to and able to form interaction with DAL-1 (Fig. 1*C*). Hence, this would be the minimal binding motif for TLSC1 binding to DAL-1.

The buried surface area of the peptide is 442.7 Å^2 as calculated by the Protein Interfaces, Surfaces, and Assemblies service (36), and there are a variety of hydrogen bonds, a salt bridge, and van der Waals interactions contributing to the binding of the TSLC1 peptide and DAL-1. The only salt bridge formed by the peptide involves Glu^{410} carboxyl oxygens and the His^{384} N$^{\epsilon 2}$ and Arg^{388} guanidinium group. The majority of hydrogen bonds are between backbone carbonyl

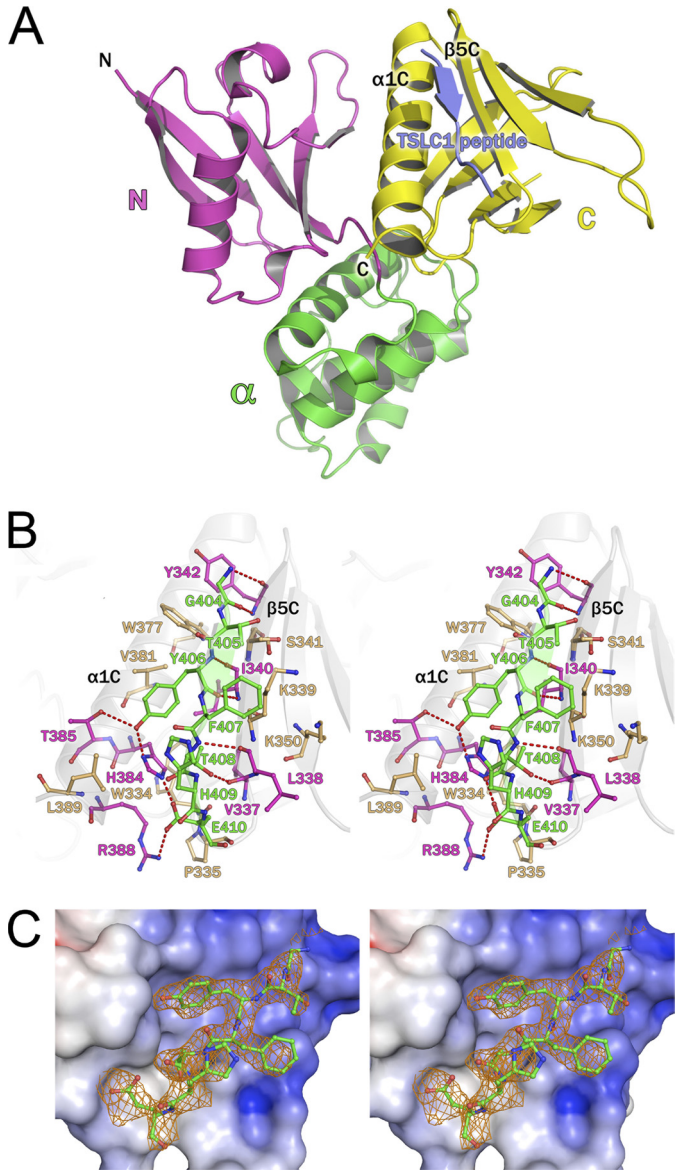

FIGURE 1. *A*, overall structure of DAL-1·TSLC1 peptide complex. Ribbon representation of the DAL-1 FERM domain bound to the TSLC1 peptide (*blue*). The DAL-1 FERM domain consists of an N-lobe (purple), α-lobe (*green*), and a C-lobe (*yellow*). The TSLC1 peptide binds in a cleft between helix α1C and β-strand β5C. *B*, TSLC1 peptide binding to the C-lobe of the DAL-1 FERM domain. Stereo image of TSLC1 peptide (*green*) binding detailing molecular interactions. The peptide forms a β-strand in association with main chain-main chain hydrogen bonds (*dashed red lines*) with β5C residues. A salt bridge exists between Arg^{338} and Glu^{410}. Tyr^{406} binds in a hydrophobic pocket and is hydrogen bonded to His^{384} and Tyr^{385}. The DAL-1 residues with hydrogen bonds are colored in *purple*. Those residues with only hydrophobic interaction with the peptide are *tan*. *C*, OMIT map of the TSLC1 peptide bound to DAL-1 with protein surface showing the electrostatic surface potential of the binding site in stereo. Electron density is contoured at 2σ at 2.3 Å resolution. Phases from the refined model with the TSLC1 peptide coordinates deleted are shown. The protein surface is colored based on the electrostatic calculations of APBS (34) where *blue* is positive and *red* is negative.

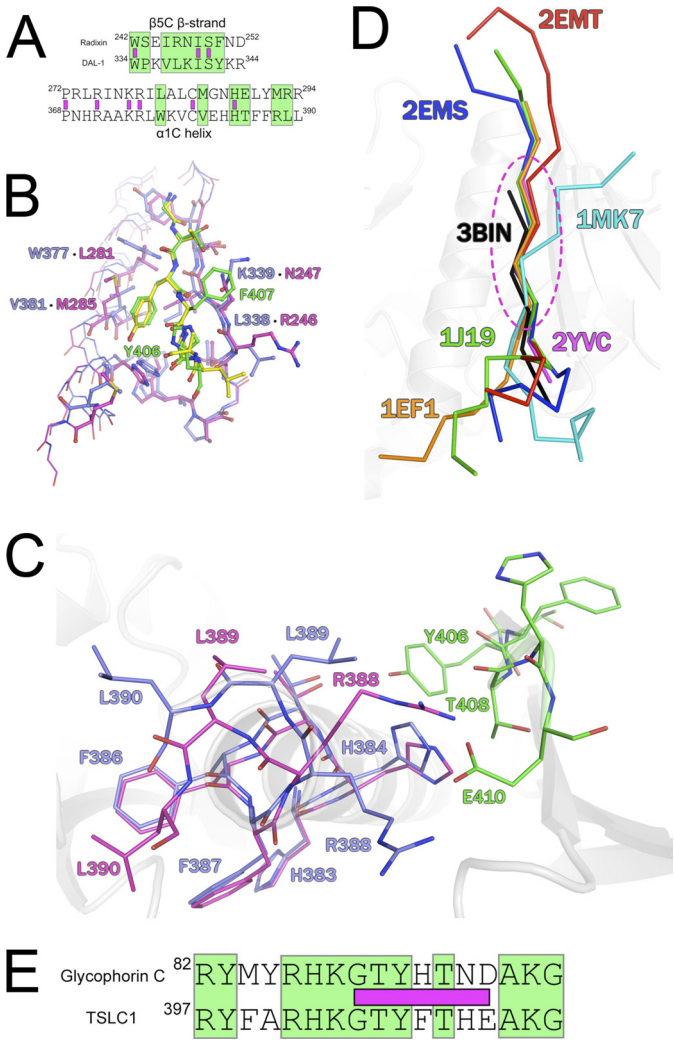

FIGURE 2. *A*, structural sequence alignment of radixin and DAL-1 β5C strand and α1C helix. *Green boxes* designate DAL-1/TSLC1 interacting residues, and *purple boxes* indicate identical residues. *B*, comparison of radixin (*purple*) and ICAM-2 (*yellow*) with DAL-1 (*blue*) and TSLC1 (*green*) in the binding pocket. Labeled residues are different between the proteins, offering a specific fit for the ICAM-2 and TSLC1 peptides. Interacting residues within the binding site are presented in stick figure representation. *C*, C-terminal domain rearrangement upon peptide binding. DAL-1 apo (*blue*) residues Arg^{388}, Leu^{389}, and Leu^{390} undergo significant movement upon peptide (*green*) binding to allow for a Glu^{410} and Arg^{388} salt bridge to form. The DAL-1·TSLC1 structure is in *purple*. *D*, core binding region of FERM domain. Superposition of peptides bound in the same region of other FERM domains. Peptides are colored according to Protein Data Bank code and in ribbon format. The FERM domains are of radixin (2YVC, 1J19, 2EMS, 2EMT), moesin (1EF1), talin (1MK7), and DAL-1 (3BIN). Residues within the *dotted oval* define the core and show minimal displacement as compared with the N- and C-terminal ends of the peptides. *E*, sequence alignment of proposed 4.1R binding region of GPC and DAL-1 binding TSLC1 peptide. *Green boxes* designate identical residues, and *purple boxes* indicate the visible binding residues of the TSLC1 peptide in the DAL-1·TSLC1 crystal structure.

and nitrogens, which assist in forming the β-sheet. There are four such main chain-main chain bonds stabilizing the interaction with the peptide and β5C. Additionally, there is a hydrogen bond between Thr^{408} $O^{\gamma 1}$ and the main chain Val^{337} carbonyl. The Tyr^{406} side chain forms a hydrogen bond to a highly conserved histidine among ERM proteins, His^{384}. All of the peptide residues are involved in van der Waals interactions. Tyr^{406} and Thr^{408}, are almost completely buried (>90%) and bind in a conserved hydrophobic pocket defined by residues Ile^{340}, His^{384}, Val^{381}, and Val^{337}. Sole contributors in helix α1C and β-strand β5C to hydrophobic interactions to the peptide include Trp^{334}, Pro^{335}, Lys^{339}, Ser^{341}, Lys^{350}, Trp^{377}, Val^{381}, and Leu^{389}. Phe^{407} is solvent exposed and packs with Lys^{339}. His^{409} of the TSLC1 peptide is mostly exposed to solvent and is involved in minimal hydrophobic contacts.

DAL-1 Structural Similarity to Radixin at Binding Site—The FERM domain of radixin, an ezrin/radixin/moesin protein, shows high homology (>82%) to DAL-1 and has been shown to bind inositol-(1,4,5)-trisphosphate, ICAM-2, an immunoglobulin membrane protein, P-selectin glycoprotein ligand-1, Na^+/H^+ exchanger regulatory factor, neutral endopeptidase 24.11, CD43, and CD44 (18, 37–42). The TSLC1 peptide that is bound to DAL-1 binds to it in a similar manner as compared with the peptides of P-selectin glycoprotein ligand-1, ICAM-2, neutral endopeptidase 24.11, and CD43, which bind to radixin. The binding pocket is defined by residues in the α1C helix and β-strand β5C. There are a number of strictly conserved residues within this region among radixin and DAL-1 (Fig. 2*A*). Specifically, within the β5C strand, there are three identical residues that are involved in interactions with the TSLC1 peptide, Trp^{334}, Ile^{340}, and Ser^{341}. Likewise, the α1C helix contains six residues identical to that of the same helix in radixin, but only one of these, His^{384}, is involved in interactions with the TSLC1 peptide.

The binding pocket and peptide-binding mode are very similar in DAL-1, radixin, moesin, and talin. In fact, the ICAM-2 peptide binds in a highly similar fashion when aligned with main chain atoms of the TSLC1 peptide (residues 5–9), with a root mean square deviation of 0.38 Å (Fig. 2*B*). Five of the seven residues (5–9) of the TSLC1 peptide form the core of binding interactions. These core interactions are similarly shared by the ICAM-2, P-selectin glycoprotein ligand-1, neutral endopeptidase 24.11, and CD43 peptides bound to radixin (37–39, 41), F-actin binding segment and integrin β3 bound to moesin (19) and talin (17), respectively (Fig. 2*D*).

Key Residues in Specificity of Binding TSLC1—As described previously, a majority of interactions are between β5C and the TSLC1 peptide. Of these interactions, those that are significantly different from that of the radixin/ICAM-2 binding site involve DAL-1 residues Leu^{338}, Lys^{339}, Trp^{377}, and Val^{381} (Fig. 2*B*). Phe^{407} is oriented toward the solvent and packs with Lys^{339}. In radixin, this residue is a small polar amino acid, Asn^{247}. It is likely this interaction would not result in favorable interactions with the TSLC1 peptide due to the hydrophobic character of Phe^{407}. In the ICAM-2 peptide, the residue corresponding to Phe^{407} is a glycine that is not involved in interacting with Asn^{247}. Tyr^{406} of the TSLC1 peptide is oriented similarly to that of the corresponding tyrosine in the ICAM-2 peptide. TSLC1 binds in the hydrophobic pocket defined by Val^{381} and Trp^{377}. In radixin, this pocket is created by the corresponding residues, Met^{285} and Leu^{281}. In both peptides, the tyrosine packs to this hydrophobic patch and interacts with the conserved histidine via a hydrogen bond. This hydrogen bond is likely a determinant factor in specific binding of the peptide, with the changes in the hydrophobic

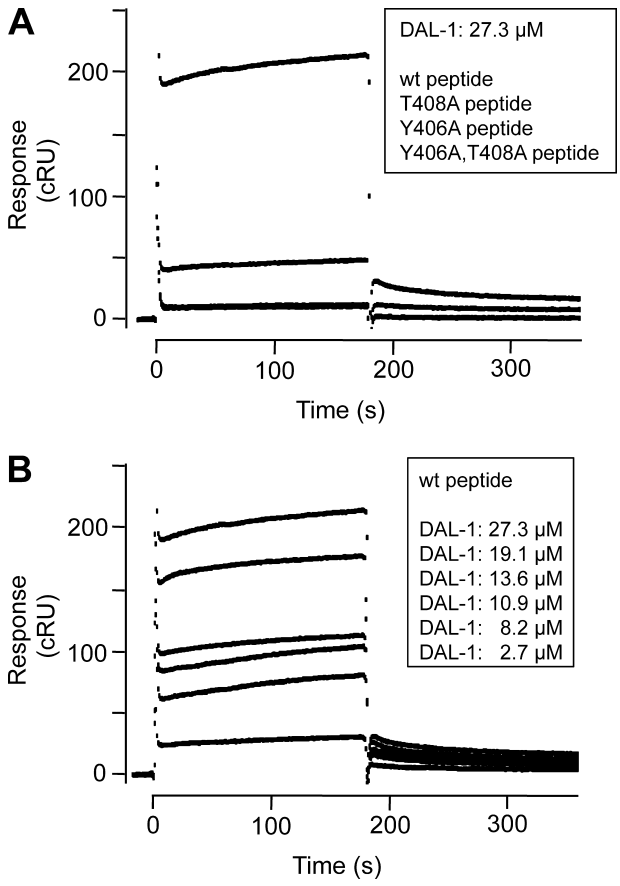

FIGURE 3. **Surface plasmon resonance-based analysis of DAL-1 binding to TSLC1 peptides.** Sensorgrams were recorded with a BIAcore 2000 instrument. Biotinylated TSLC1 peptides were immobilized on streptavidin chips, and various concentrations of DAL-1 were analyzed in HBS, 0.005% P20, 0.5 mM TCEP, 0.5 M betaine. Corrected responses (*cRU*) were obtained by subtracting the response in the reference lane (scrambled peptide). *A*, corrected responses of DAL-1 (27.3 μM) injected in lanes containing WT peptide (*top* sensorgram), T408A peptide (intermediate sensorgram), Y406A peptide (bottom sensorgram) and Y406A,T408A peptide (*bottom* sensorgram), respectively. Note that the responses in the Y406A and the Y406A,T408A double-mutant peptide lanes were identical, giving completely superimposed sensorgrams. *B*, corrected responses of various concentrations (27.3–2.7 μM, from *top* to *bottom*) of DAL-1 on WT peptide.

character of this region being less significant. TSLC1 varies from the FERM domain Motif-1 (R*xx*TY*x*V*xx*A) of the ICAM-2 peptide (38) in that the valine is a threonine. It was previously suggested that this residue was required to be small and hydrophobic. In the present DAL-1·TSLC1 complex structure, Thr^{408} forms a stabilizing hydrogen bond to the main chain carbonyl of DAL-1 Val^{337} at the same time as its Cγ packs into a hydrophobic pocket. Only a threonine in this position can play these dual roles.

Surface Plasmon Resonance Binding Analysis of DAL-1·TSLC1 Peptides—From the present co-crystal structure, it is apparent that Tyr^{406} and Thr^{408} are likely critical in TSLC1 binding to DAL-1. To confirm this, we studied the binding of DAL-1 to both WT and mutant TSLC1 peptide sequences using surface plasmon resonance. The WT peptide showed a specific binding that was almost completely abolished both in the double mutant and single mutant peptides, in which Tyr^{406} and Thr^{408}, or Tyr^{406} alone, were mutated to Ala residues (Fig. 3*A*). A small but significant binding remained when Thr^{408} alone was mutated (Fig. 3*A*). This confirms the critical roles of Tyr^{406} and Thr^{408} in the TSLC1 binding to DAL-1, in agreement with the hypothesis derived from the structural data. Varying the DAL-1 concentrations showed the expected concentration dependence of the binding to the WT peptide (Fig. 3*B*). The sensorgram profiles indicated a complex binding reaction with some interesting features. The dominating reaction was characterized by an almost instant complex formation and dissociation (Fig. 3*B*). On top of that, a much slower reaction occurred. Comparison of the WT peptide-binding profiles with the mutant peptide-binding profiles indicated that the dominating rapid association/dissociation represented the primary binding between the TSLC1 WT peptide and the DAL-1 FERM domain. The slow, superimposed reaction could represent a conformation change in the complex after its formation. This would be in agreement with the observed conformation change in the crystal structure of DAL-1 upon peptide binding, in which Arg^{388} in the binding pocket moves 5.8 Å (Fig. 2*C*). Therefore, we analyzed the sensorgrams by the two-state reaction model in BIAevaluation 4.1, in which the second state represents a conformation change in the complex after its formation.

This yielded a good global curve fit from which the binding association and dissociation rate constants of the primary complex formation, k_{a1} and k_{d1}, were determined to be $6.7 \times 10^{-1} \pm 6 \times 10^{-3}$ M^{-1} s^{-1} and $4.7 \times 10^{-4} \pm 3 \times 10^{-6}$ s^{-1} (mean ± S.E.), respectively, which in turn gave the equilibrium dissociation constant $K_{D1} = k_{d1}/k_{a1} = 7.1 \times 10^{-4}$ M. The rate constants of the second reaction were $k_{a2} = 1.0 \times 10^{-4} \pm 3.4 \times 10^{-4}$ s^{-1}, and $k_{d2} = 1.2 \times 10^{-7} \pm 1 \times 10^{-9}$ s^{-1}, respectively. Although the large standard error in k_{a2} gives a very uncertain value of $K_{D2} = k_{d2}/k_{a2}$, the results indicate that the apparent overall dissociation equilibrium constant, $K_{D1} \times K_{D2}$, was in the order of $10^{-6} - 10^{-7}$ M. Because the rapid association of the primary binding indicated that binding equilibrium of this reaction was reached during the injection phase, we could also calculate the equilibrium constant of the primary binding, K_{D1}, directly from the corrected sensorgrams. This gave a K_{D1} of 10×10^{-4} M, which is thus in good agreement with the K_{D1} (7.1×10^{-4} M) calculated from the global curve fitting to the two-state reaction model. These analyses thus show that the binding interaction between TSLC1 and DAL-1 is of rather low affinity. However, adhesion receptors that are engaged in cell-cell binding cluster in the cell contact regions, giving rise to high local concentrations. Therefore, also low affinity interactions can result in significant complex formation in localized regions of the plasma membrane.

Implications for Binding Mode of Protein 4.1R to Glycophorin C—The glycophorin C (GPC) cytoplasmic domain interacts with protein 4.1R. The interaction was proposed to be in the α-lobe based on resonant mirror detection and mutant constructs with exons removed (43) in combination with the electrostatic character of the surface in the α-lobe on the 4.1R protein (15). However, a recent NMR study of the 4.1R protein α-lobe showed only small interactions on the fast exchange time scale even with 10-fold excess of GPC C-terminal peptide (44). Interestingly, the binding region of GPC displays

strong sequence similarity to the cytoplasmic domain of TSLC1 as determined by BLAST (45) (Fig. 2*E*). Accordingly, based on the structural evidence presented here of TSLC1 binding to DAL-1 and other FERM domains binding to similar peptides in the C-lobe and the very weak interactions of even large excess of ligand in the α-lobe, the binding site for GPC is most likely in the C-lobe also in the case of protein 4.1R.

It is intriguing to speculate that TSLC1 binding to DAL-1 offers a way to restrict or enhance binding of proteins that bind to the lateral membrane. Obviously, there are a variety of interactions involved in these critical areas that, when disrupted, can result in metastasis. It will be interesting to see what other proteins may be involved with DAL-1 and their effects on tumor suppression in a variety of cancers.

Acknowledgments—We thank Elspeth Gordon and David R. Hall for technical support at beamline ID23.1 and ID14.4 at the European Synchrotron Radiation Facility.

REFERENCES

1. Hynes, R. O. (1999) *Trends Cell Biol.* **9,** M33–37
2. Benson, D. L., Schnapp, L. M., Shapiro, L., and Huntley, G. W. (2000) *Trends Cell Biol.* **10,** 473–482
3. Takai, Y., Irie, K., Shimizu, K., Sakisaka, T., and Ikeda, W. (2003) *Cancer Sci.* **94,** 655–667
4. Watabe, K., Ito, A., Koma, Y. I., and Kitamura, Y. (2003) *Histol. Histopathol.* **18,** 1321–1329
5. Kuramochi, M., Fukuhara, H., Nobukuni, T., Kanbe, T., Maruyama, T., Ghosh, H. P., Pletcher, M., Isomura, M., Onizuka, M., Kitamura, T., Sekiya, T., Reeves, R. H., and Murakami, Y. (2001) *Nat. Genet.* **27,** 427–430
6. Lung, H. L., Cheung, A. K., Xie, D., Cheng, Y., Kwong, F. M., Murakami, Y., Guan, X. Y., Sham, J. S., Chua, D., Protopopov, A. I., Zabarovsky, E. R., Tsao, S. W., Stanbridge, E. J., and Lung, M. L. (2006) *Cancer Res.* **66,** 9385–9392
7. Surace, E. I., Strickland, A., Hess, R. A., Gutmann, D. H., and Naughton, C. K. (2006) *J. Androl.* **27,** 816–825
8. Masuda, M., Yageta, M., Fukuhara, H., Kuramochi, M., Maruyama, T., Nomoto, A., and Murakami, Y. (2002) *J. Biol. Chem.* **277,** 31014–31019
9. Mao, X., Seidlitz, E., Ghosh, K., Murakami, Y., and Ghosh, H. P. (2003) *Cancer Res.* **63,** 7979–7985
10. Yageta, M., Kuramochi, M., Masuda, M., Fukami, T., Fukuhara, H., Maruyama, T., Shibuya, M., and Murakami, Y. (2002) *Cancer Res.* **62,** 5129–5133
11. Tran, Y. K., Bögler, O., Gorse, K. M., Wieland, I., Green, M. R., and Newsham, I. F. (1999) *Cancer Res.* **59,** 35–43
12. Bernkopf, D. B., and Williams, E. D. (2008) *Expert Opin Ther. Targets* **12,** 845–853
13. Diakowski, W., Grzybek, M., and Sikorski, A. F. (2006) *Folia Histochem Cytobiol.* **44,** 231–248
14. Chishti, A. H., Kim, A. C., Marfatia, S. M., Lutchman, M., Hanspal, M., Jindal, H., Liu, S. C., Low, P. S., Rouleau, G. A., Mohandas, N., Chasis, J. A., Conboy, J. G., Gascard, P., Takakuwa, Y., Huang, S. C., Benz, E. J., Jr., Bretscher, A., Fehon, R. G., Gusella, J. F., Ramesh, V., Solomon, F., Marchesi, V. T., Tsukita, S., Tsukita, S., Hoover, K. B., *et al.* (1998) *Trends Biochem. Sci.* **23,** 281–282
15. Han, B. G., Nunomura, W., Takakuwa, Y., Mohandas, N., and Jap, B. K. (2000) *Nat. Struct. Biol.* **7,** 871–875
16. Ceccarelli, D. F., Song, H. K., Poy, F., Schaller, M. D., and Eck, M. J. (2006) *J. Biol. Chem.* **281,** 252–259
17. García-Alvarez, B., de Pereda, J. M., Calderwood, D. A., Ulmer, T. S., Critchley, D., Campbell, I. D., Ginsberg, M. H., and Liddington, R. C. (2003) *Mol. Cell* **11,** 49–58
18. Hamada, K., Shimizu, T., Matsui, T., Tsukita, S., and Hakoshima, T. (2000) *EMBO J.* **19,** 4449–4462
19. Pearson, M. A., Reczek, D., Bretscher, A., and Karplus, P. A. (2000) *Cell* **101,** 259–270
20. Shimizu, T., Seto, A., Maita, N., Hamada, K., Tsukita, S., Tsukita, S., and Hakoshima, T. (2002) *J. Biol. Chem.* **277,** 10332–10336
21. Smith, W. J., Nassar, N., Bretscher, A., Cerione, R. A., and Karplus, P. A. (2003) *J. Biol. Chem.* **278,** 4949–4956
22. The Uniprot Consortium (2010) *Nucleic Acids Res.* **38,** D142–D148
23. Yu, T., Robb, V. A., Singh, V., Gutmann, D. H., and Newsham, I. F. (2002) *Biochem. J.* **365,** 783–789
24. Singh, V., Miranda, T. B., Jiang, W., Frankel, A., Roemer, M. E., Robb, V. A., Gutmann, D. H., Herschman, H. R., Clarke, S., and Newsham, I. F. (2004) *Oncogene* **23,** 7761–7771
25. Nunomura, W., Takakuwa, Y., Parra, M., Conboy, J. G., and Mohandas, N. (2000) *J. Biol. Chem.* **275,** 6360–6367
26. Ericsson, U. B., Hallberg, B. M., Detitta, G. T., Dekker, N., and Nordlund, P. (2006) *Anal. Biochem.* **357,** 289–298
27. Collaborative Computational Project, N. (1994) *Acta Crystallogr. D. Biol. Crystallogr.* **50,** 760–763
28. McCoy, A. J., Grosse-Kunstleve, R. W., Adams, P. D., Winn, M. D., Storoni, L. C., and Read, R. J. (2007) *J. Appl. Crystallogr.* **40,** 658–674
29. Kabsch, W. (1993) *J. Appl. Crystallogr.* **26,** 795–800
30. Murshudov, G. N., Vagin, A. A., and Dodson, E. J. (1997) *Acta Crystallogr. D. Biol. Crystallogr.* **53,** 240–255
31. Emsley, P., and Cowtan, K. (2004) *Acta Crystallogr. D. Biol. Crystallogr.* **60,** 2126–2132
32. Delano, W. L. (2002) *The PyMOL Molecular Graphics System*, DeLano Scientific, Palo Alto, CA
33. Landau, M., Mayrose, I., Rosenberg, Y., Glaser, F., Martz, E., Pupko, T., and Ben-Tal, N. (2005) *Nucleic Acids Res.* **33,** W299–302
34. Baker, N. A., Sept, D., Joseph, S., Holst, M. J., and McCammon, J. A. (2001) *Proc. Natl. Acad. Sci. U.S.A.* **98,** 10037–10041
35. Krissinel, E., and Henrick, K. (2004) *Acta Crystallogr. D. Biol. Crystallogr.* **60,** 2256–2268
36. Krissinel, E., and Henrick, K. (2007) *J. Mol. Biol.* **372,** 774–797
37. Takai, Y., Kitano, K., Terawaki, S., Maesaki, R., and Hakoshima, T. (2008) *J. Mol. Biol.* **381,** 634–644
38. Hamada, K., Shimizu, T., Yonemura, S., Tsukita, S., Tsukita, S., and Hakoshima, T. (2003) *EMBO J.* **22,** 502–514
39. Takai, Y., Kitano, K., Terawaki, S., Maesaki, R., and Hakoshima, T. (2007) *Genes Cells* **12,** 1329–1338
40. Terawaki, S., Maesaki, R., and Hakoshima, T. (2006) *Structure* **14,** 777–789
41. Terawaki, S., Kitano, K., and Hakoshima, T. (2007) *J. Biol. Chem.* **282,** 19854–19862
42. Mori, T., Kitano, K., Terawaki, S., Maesaki, R., Fukami, Y., and Hakoshima, T. (2008) *J. Biol. Chem.* **283,** 29602–29612
43. Nunomura, W., Takakuwa, Y., Parra, M., Conboy, J., and Mohandas, N. (2000) *J. Biol. Chem.* **275,** 24540–24546
44. Kusunoki, H., and Kohno, T. (2009) *Proteins* **76,** 255–260
45. Altschul, S. F., Madden, T. L., Schäffer, A. A., Zhang, J., Zhang, Z., Miller, W., and Lipman, D. J. (1997) *Nucleic Acids Res.* **25,** 3389–3402